IMPROVED CORTICAL THICKNESS MEASUREMENT FROM MR IMAGES USING PARTIAL VOLUME ESTIMATION

Pierrick Bourgeat[1], *Oscar Acosta*[1]
Maria Zuluaga[1], *Jurgen Fripp*[1], *Olivier Salvado*[1]

[1]Australian e-Health Research Centre,
CSIRO ICT Centre, Brisbane, Australia.

Sébastien Ourselin[1,2]

[2]Centre for Medical Image Computing,
University College London,
Gower St, London, WC1E 6BT, UK.

ABSTRACT

Accurate cortical thickness estimation is important for the study of many neurodegenerative diseases. Amongst the approaches previously proposed in the literature, mesh based techniques typically lack computational efficiency, whereas voxel based techniques tend to be faster but are less accurate. The aim of this work is to propose a novel voxel based method using the Laplacian definition of thickness, being both accurate and computationally efficient. A subvoxel estimate of the location of the boundary is obtained through ray-casting using both partial volume estimation and the direction of the streamlines. This estimate is then used to initialise the boundary conditions when computing the length of the streamlines. The approach was validated on synthetic phantoms and real data, showing an improved accuracy and reproducibility.

Keywords: gray matter segmentation, cortical thickness, partial volume estimation.

1. INTRODUCTION

Measurement of cortical thickness from 3D magnetic resonance (MR) images can aid diagnosis and longitudinal studies of a wide variety of neurodegenerative diseases. Manual measurements are labour intensive and have a high variability, which implies a need for accurate and automated software that maps the three dimensional cortical thickness of the entire brain volume. Amongst the numerous approaches previously proposed in the literature, the two emerging trends are the mesh based and voxel based techniques. Mesh based approaches have the advantage to operate in the continuous spatial domain and therefore can achieve subvoxel resolution. Most implementation also include a smoothness constraint which provides robustness to noise and false edges. This however come to a cost as these approaches have typical running time of over 20 hour on standard PC [1]. Following the surface extraction, the thickness estimation can be performed using several sets of metric [2]. In contrast, voxel based techniques operate directly on the 3D voxel grid of the image, and therefore are more computationally efficient but are hampered by their limited accuracy. They are also less robust to noise and missegmentation as they typically lack the mechanisms required to assess and correct topological errors. Several approaches have been proposed for thickness estimation and the definition based on Laplace equation, first introduced by Jones [3], has gained wide acceptance. The Laplace's equation associates two points on the opposite cortical boundaries and defines thickness between them. Whereas Jones' approach [3] explicitly traces streamlines (Lagrangian approach), Yezzi [4] proposed a more efficient method which involves solving a pair of first order linear partial differential equations without any explicit construction of correspondences (Eulerian approach). The major drawback of the Eulerian approach is the accuracy of the thickness estimation, especially within thin structures. An hybrid Eulerian-Lagrangian approach was recently proposed by Rocha [5] to improve accuracy while preserving efficiency but still lacks the accuracy required for clinical applications, as both approaches do not allow for subvoxel initialisation at tissues boundaries. In this paper, we propose to improve the hybrid Eulerian-Lagrangian approach. The partial volume (PV) content of each boundary voxel, combined with the direction of the tangent field, is used to accurately measure the position of the boundary through ray-casting. This measurement provides a subvoxel initialisation for the Eulerian approach. Using PV model, gray matter mask can be restricted to pure voxels only, which improves the segmentation of deep sulci while preserving the accuracy of the thickness estimation. For the remainder of the paper, we first describe the segmentation algorithms used, followed by the partial volume estimation, and the cortical thickness estimation. We then validate the accuracy of our approach on synthetic data, and its reproducibility on real data.

2. METHODS

2.1. Brain Segmentation.

Based on the previously proposed expectation maximisation segmentation (EMS) algorithm [6], we have implemented a method for segmentation of brain tissues into gray matter (GM), white matter (WM) and cerebrospinal fluid (CSF), which in-

cludes a polynomial based bias field correction and Markov random fields to reduce the effects of noise [7]. In this paper, the priors are first affinely registered to the data using a robust block matching approach [8], followed by a smooth B-spline based non-rigid registration [9] using normalised mutual information [10]. The registration is performed on a 20mm spacing grid, producing a smooth deformation field. The registered priors are then used to initialise the EMS and enforce spatial consistency throughout the segmentation process.

2.2. Partial Volume Estimation

Partial volume along tissue interfaces is estimated by modeling mixture of pure tissues and performing a maximum a posteriori classification. We adopted a two stage procedure [11] relying on both intensity and spatial information [12]. This scheme has been optimised to compute a single map containing the fractional content of pure gray matter using the hard segmentations and bias corrected images obtained after the EMS algorithm. Since voxels containing PV are mostly present along boundaries, PV evaluation is first restricted to the region formed by a dilated gray matter mask (radius 4), followed by a segmentation performed using a Potts model [12] and optimised with the Iterative Condition Modes algorithm [13]. Fractional content $F_{j/k}$ between tissue j and k is then computed following Santago and Gage technique [14] using the bias corrected intensity $\bar{x}_i$, and the means of the two pure tissue types μ_j and μ_k, such that:

$$F_{j/k} = U\left(\frac{\mu_j - \bar{x}_i}{\mu_j - \mu_k}\right) \tag{1}$$

where $U(\cdot)$ is a limiter restricting the range of the fractional content to $[0, 1]$. The partial volume coefficient (PVC) of GM, is defined as:

$$\text{GMPVC} = F_{\text{GM/WM}} \cup F_{\text{GM/CSF}} \tag{2}$$

2.3. Thickness using fractional content values

The thickness is measured using the approach of Jones [3] where Laplace's equation is solved in the GM volume (with the WM and CSF voxels adjacent to the boundaries of the GM set to fixed potentials) such that:

$$\nabla^2 f(x, y, z) = \frac{\partial^2 f}{\partial x^2} + \frac{\partial^2 f}{\partial y^2} + \frac{\partial^2 f}{\partial z^2} = 0 \tag{3}$$

The solution $f(x, y, z)$ is a scalar field which divides the cortex into a set of equipotential sublayers (Fig. 1.a). The normalised gradient of the Laplace solution provides streamlines between the WM and CSF, which do not intersect, are locally perpendicular to the equipotential sublayers, and provide a unique correspondence between the two boundaries. The tangent vectors of the correspondence trajectories $\overrightarrow{T}$ corresponds to the normalised gradient vector field of $f(\mathbf{x})$, regularised using a Gaussian function G_σ with $\sigma = 1$ such that

$$\overrightarrow{T} = G_\sigma * \frac{\nabla f}{\|\nabla f\|}. \tag{4}$$

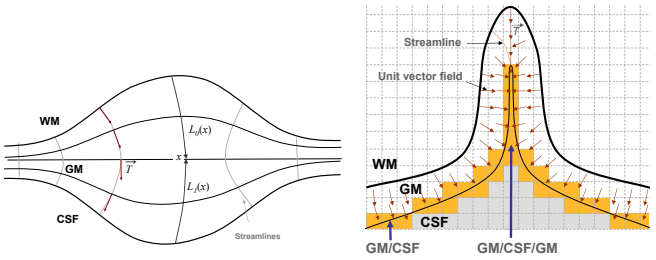

(a) (b)

Fig. 1. **a.** Distance equations L_0 and L_1 for computation of thickness W at a given point $\mathbf{x}$. **b.** PV voxels (GM/CSF) in deep sulci. Some of the voxels are composed of a mixture GM/CSF/GM (GM in opposite directions). For those voxels, initialisation of distance functions following the tangent field is ambiguous.

An explicit integration of $\overrightarrow{T}$ ($-\overrightarrow{T}$, resp.) between $\mathbf{x}$ and the CSF (WM resp.) following the streamlines as proposed by Jones [3], can be performed to compute the length of the streamlines $L_1(\mathbf{x})$ ($L_0(\mathbf{x})$resp.). This approach, called Lagrangian, is computationally expensive since each trajectory is explicitly traced. In a further work, Yezzi [4] proposed an Eulerian approach, in which a pair of first order partial differential equations are solved to compute the length ($L_1(\mathbf{x})$ and $L_0(\mathbf{x})$) of the trajectories without explicitly tracking the streamlines:

$$\nabla L_0 \cdot \overrightarrow{T} = 1 \quad \text{and} \quad -\nabla L_1 \cdot \overrightarrow{T} = 1, \tag{5}$$

with boundary conditions $L_0(\mathbf{x}) = 0, L_1(\mathbf{x}) = 0, \forall \mathbf{x} \in [\text{WM}, \text{CSF}]$, leading to numerical finite difference approximations for $L_0[x, y, z]$ and $L_0[x, y, z]$ [4]). Rocha [5] showed that the main advantage of the Eulerian approach is the computational speed. However, its major drawback is the accuracy whose effects are emphasised when the anatomical structures, such as the GM, are small compared to the spatial resolution.

On these thin structures, the most important factor affecting the accuracy of the Eulerian approach is the choice of initial boundary conditions for L_0 and L_1. In [4] they are fixed to 0, implicitly assuming that the boundaries coincide with the centre of the grid points and yielding to an overestimation of the thickness when L_0 and L_1 are summed. Initialisation of the boundaries to half of the negative mean voxel spacing (*i.e.* -0.5 for 1mm spacing isotropic images) as proposed by Diep [7], produces the correct thickness but only for isotropic images when the boundaries coincide with the voxels borders (no PV effect) and are aligned with the grid. For small and highly convoluted structures, such as the GM where PV effects become preponderant, this initialisation hamper greatly the accuracy. Rocha [5] improved the boundary conditions by defining boundaries from a presegmented surface computed with subvoxel accuracy. To our knowledge, none of the previously proposed methods addresses the initialisation problem within a pure discrete voxel-based scheme.

2.3.1. Correction of segmentation.

The accuracy of the measure will depend on the quality of the GM segmentation and we first produce a reliable 3D bounded GM grid for thickness computation. This grid is contiguous along the interfaces allowing solving the PDE from one tissue boundary (GM/WM) to the other (GM/CSF). To this end, the GMPVC map is combined with the obtained hard segmentations as follows:

- Every GM voxel belonging to the GM/CSF (GM/WM resp.) boundary is reclassified as CSF (WM resp.) if the GMPVC is below 1.
- To guarantee continuity of the GM grid, all the CSF (WM resp.) voxels lying on a CSF/WM boundary are reclassified as GM, regardless of their fractional content.

Restricting the GM mask to only pure tissue voxels provides a good delineation of deep sulci. Furthermore, correcting for the WM/CSF gaps allows us to measure thin GM zones, even when its thickness is less than one voxel.

2.3.2. Boundaries initialisation.

To define the boundary condition, for each GM voxel sharing a boundary with one or more mixed voxel we follow the streamline from the GM boundary in the direction of $\overrightarrow{T}$ ($-\overrightarrow{T}$ resp.), looking for the real boundary GM/CSF (GM/WM resp.) where the GM fractional content equals the CSF (WM resp.) fractional content. The boundary point x_0 can be detected by trilinear interpolation within the neighbouring voxels in the GMPVC map, achieving subvoxel resolution. A ray casting technique [15] is used to extend the streamlines until the actual boundary is found within the GMPVC map. The implementation is based on a dichotomy search, with decreasing stepsize down to $\epsilon = 1/10^{-3}$ of the voxel size.

Unlike Yezzi's approach [4], where the boundary conditions was set for all voxels labelled as WM or CSF, we set the boundary condition to the GM voxels sharing a boundary with one or more mixed voxel, as $\overrightarrow{T}$ is undefined outside the GM mask. Also, as depicted in Fig. 1.b, it is quite common for deep sulci to have a CSF voxel surrounded by GM, which means that at this voxel the computed fractional content of GM (GM/CSF/GM) does not reflect the geometry of the structure. Therefore, the GMPVC map is modified according to the direction of the streamlines at the boundary. If a mixed GM/CSF voxel is surrounded by two or more GM voxels with their unit tangent vectors $\overrightarrow{T}$ pointing in opposite directions, the GMPVC value is reapportioned amongst the adjacent voxels according to the projection of their unit tangent vector $\overrightarrow{T}$ over the rectangular grid, such that for x :

$$\begin{aligned} \text{GMPVC}(i) = \text{GMPVC}(i) \frac{1}{1 + \frac{|T_x[i-1]| + |T_x[i+1]|}{2}} \\ if \quad sign(T_x[i-1]) \neq sign(T_x[i+1]) \end{aligned} \tag{6}$$

which is equivalent to reapportion the fractional content amongst the voxels $i-1$ and $i+1$. This step is reiterated for each direction y, z on the discrete grid coordinates j, k, ensuring that the PVC volume at this voxel will be equally distributed to all neighbouring GM voxels.

Lastly, when the segmentation is corrected, some WM and CSF voxels are assigned to the GM mask, which results in some GM voxels having a GMPVC<1. Since a PVC=0.5 correspond to the real boundary passing through the centre of the voxel, the value of the GMPVC needs to be considered when casting the ray, searching for the actual boundary. Therefore, If the GMPVC drops below 0.5, the direction of the ray cast needs to be inverted to point toward the GM, instead of pointing toward the mixed voxels.

With both boundaries initialised, the PDE are solved in the remaining GM grid using the Eulerian approach [4] generalised for anisotropic images [7]. The cortical thickness map is then smoothed using the interquartile mean (IQM) within a 5mm radius sphere. The smoothing is performed on the WM/GM boundary, and restricted to the connected components of the GM mask inscribed within the smoothing sphere. Using the deformation field previously computed to match the priors to the data, the automated anatomical labelling (AAL) template is mapped to the native space of the patient allowing to compute the mean thickness for each region of interest (ROI).

3. EXPERIMENTS AND RESULTS

3.1. Spherical shell

Experiments over a 3mm thick hollow sphere were performed to determine the accuracy of the thickness measurement using PV estimation. To simulate the PV, the binary phantoms are first generated on a high resolution grid ($N \times N \times N$, with $N = 1100$) with 0.1mm^3 spacing and resampled to a given lower resolution similar to actual MRI. The value of each voxel is defined by the percentage of non-zero voxels within the region covered by this voxel on the original grid.

The comparison of the thickness estimation method with and without using PV estimation over spherical shells is presented in Table 1. The errors caused by the PV effect on the sphere mean thickness are significantly reduced when using PV estimation. For a 1mm^3 resolution image the error is reduced from 9.33% to 1.33%. The results also show that the PV estimation produces accurate results for both isotropic and anisotropic data and accuracy is proportional to the image resolution.

3.2. Real data

From the OASIS database [16], we extracted 10 young healthy subjects who underwent 4 scans at baseline and 4 more scans during a subsequent session after a short delay (less than 90 days). For each session, an average motion-corrected image

Table 1. Synthetic spherical shells 3mm thick were generated to compare accuracy of the thickness estimation with and without using PV estimation.

Resolution	No PV Estimation Mean $\pm$ SD	PV Estimation Mean $\pm$ SD
0.5x0.5x0.5	2.86 ± 0.08	3.01 ± 0.01
0.5x0.5x1	2.80 ± 0.16	3.02 ± 0.02
1x1x1	2.72 ± 0.17	3.04 ± 0.02
1x1x1.5	2.68 ± 0.24	3.05 ± 0.08

(co-registered average of all available data) is used for our reliability test. The scans are T1W MPRAGE with isotropic 1mm^3 resolution.

The Pearson correlation coefficient was used for each ROI of the AAL template to assess the correlation between the two measurements (Fig. 2.a). The cerebellum and subcortical *nuclei* were excluded from the analysis. R^2 for all the regions was above 0.8, and a paired t-test did not reveal any significant differences between the 2 measurements ($p > 0.01$). We found a mean (std. dev.) cortical thickness over the whole brain of 2.54mm(0.3mm), which is within the accepted range of cortical thickness for healthy young adults. An example of the thickness map of an AD patient is presented in Fig. 2.b showing a pattern of atrophy in the temporal and occipital lobes.

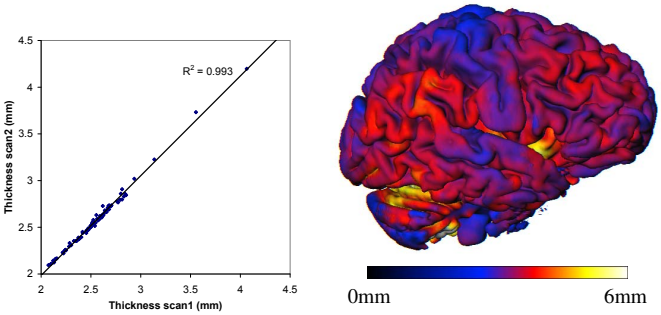

(a) (b)

Fig. 2. **a.** Mean cortical thickness over each AAL regions on two scans of the 10 subjects. **b.** Marching cube rendering of a thickness map of an AD patient after smoothing.

4. CONCLUSION

We have described a novel voxel-based method for accurate cortical thickness estimation. The main contribution with previously proposed methods is that it preserves the computational efficiency of Eulerian-PDE approaches while improving the accuracy of the Lagrangian scheme through a better initialisation. Unlike other approaches requiring a mesh to take advantage of the PV estimation, all the calculations are performed on the discrete grid. The method is simple, using a ray casting technique in the direction of the tangent field, such that the estimated boundary defines an equilibrium between the shared fractional content. The full algorithm, including atlas registration, segmentation, PV estimation, thickness estimation, smoothing and regional statistics extraction run under 30 minutes on a standard PC.

5. REFERENCES

[1] J.K. Lee, J.M. Lee, *et al.*, "A novel quantitative cross-validation of different cortical surface reconstruction algorithms using MRI phantom," *Neuroimage*, vol. 31, no. 2, pp. 572-584, 2006.

[2] J.P. Lerch and A.C. Evans, "Cortical thickness analysis examined through power analysis and a population simulation," *Neuroimage*, vol. 24, no. 1, pp. 163-173, 2005.

[3] S.E. Jones, B.R. Buckbinder, and I. Aharon, "Three-dimensional mapping of cortical thickness using Laplace's equation," *HBM*, vol. 11, no. 1, pp. 12-32, 2000.

[4] A.J. Yezzi and J.L. Prince, "An Eulerian PDE approach for computing tissue thickness," *IEEE TMI*, vol. 22, no. 10, pp. 1332-1339, 2003.

[5] K.R. Rocha, A.J. Yezzi, and J.L. Prince, "A hybrid Eulerian-Lagrangian approach for thickness, correspondence, and gridding of annular tissues," *IEEE TIP*, vol. 16, no. 3, pp. 636-648, 2007.

[6] K. van Leemput, F. Maes, *et al.*, "Automated model-based bias field correction of MR images of the brain," *IEEE TMI*, vol. 18, no. 10, pp. 885-896, 1999.

[7] T-M. Diep, P. Bourgeat, and S. Ourselin, "Efficient use of cerebral cortical thickness to correct brain MR segmentation," in *IEEE (ISBI'07)*, Washington DC, USA, 2007, pp. 592-595.

[8] S. Ourselin, A. Roche, *et al.*, "Reconstructing a 3D structure from serial histological sections," *IVC*, vol. 19, no. 1, pp. 25-31, 2001.

[9] D. Rueckert, L.I. Sonoda, *et al.*, "Nonrigid registration using free-form deformations: Application to breast MR images," *IEEE TMI*, vol. 18, pp. 712-721, 1999.

[10] C. Studholme, D.L.G. Hill, and D.J. Hawkes, "An overlap invariant entropy measure of 3D medical image alignment," *Patt. Rec.*, vol. 32, no. 1, pp. 71-86, 1998.

[11] M. Zuluaga, O. Acosta, *et al.*, "Cortical thickness measurement from magnetic resonance images using partial volume estimation," in *SPIE: IP*, San Diego, USA, 2008, vol. 6914, p. 691418.

[12] D.W. Shattuck, S.R. Sandor-Leahy, *et al.*, "Magnetic resonance image tissue classification using a partial volume model," *Neuroimage*, vol. 13, no. 5, pp. 856-876, 2001.

[13] J. Besag, "On the statistical analysis of dirty pictures," *J. of Royal Stat. Soc.*, vol. 48, pp. 259-302, 1986.

[14] P. Santago and H.D. Gage, "Quantification of MR brain images by mixture density and partial volume modeling," *IEEE TMI*, vol. 12, no. 3, pp. 566-574, 1993.

[15] J. Foley, A. Van Dam, *et al.*, *Computer Graphics: Principles and Practice*, p. 701, Addison-Wesley, 1995.

[16] D.S. Marcus, T.H. Wang, *et al.*, "Open Access Series of Imaging Studies (OASIS): Cross-Sectional MRI Data in Young, Middle Aged, Nondemented, and Demented Older Adults," *J. Cogn. Neuro.*, vol. 19, pp. 1498-1507, 2007.